IEEE Access
Multidisciplinary ⋮ Rapid Review ⋮ Open Access Journal

Received 21 October 2022, accepted 3 November 2022, date of publication 4 November 2022,
date of current version 30 November 2022.

Digital Object Identifier 10.1109/ACCESS.2022.3219852

RESEARCH ARTICLE

Instant Orientation Correction Strategy: Holonomic System-Based Decentralized Control for Nonholonomic Agents

CHANYEONG JEONG[1],[*], EUGENE KIM[1],[*], MYEONG-HWAN HWANG[1], HYO-SUNG AHN[2], (Senior Member, IEEE), AND HYUN-ROK CHA[1]

[1] Automotive Materials & Components Research and Development Group, Korea Institute of Industrial Technology, Gwangju 61012, South Korea

[2] Distributed Control and Autonomous System Laboratory, School of Mechanical Engineering, Gwangju Institute of Science and Technology, Gwangju 61005, South Korea

Corresponding author: Hyun-Rok Cha (hrcha@kitech.re.kr)

[*] Chanyeong Jeong and Eugene Kim are co-first authors.

This work was supported by the Korea Institute of Industrial Technology through the Development of Core Technologies for a Working Partner Robot in the Manufacturing Field under Grant KITECH EO-22-0009.

ABSTRACT This study proposes an instant orientation correction strategy to perform an orientation alignment-based formation control applicable to nonholonomic agents. Generally, an orientation alignment-based formation control cannot be applied to nonholonomic agents with orientation constraints because it is originally a protocol for holonomic agents. Therefore, we improved the orientation alignment-based formation control using an instant orientation correction strategy that modifies the local frame of the nonholonomic agents. To examine the effect of the proposed method, simulations and experiments using representative parameters were conducted for unicycle-modeled nonholonomic agents. As a result, nonholonomic agents could execute a holonomic system-based control law by applying the proposed correction strategy. The simulation confirmed the change in the convergence time and the cumulative error of the angular velocity according to the number of agents and the updated step size of the local desired position. As the updated step size increased, the cumulative error of the angular velocity tended to increase (0.3 rad/s∼0.4rad/s). Also, the convergence time was not dramatically affected by the update step size and the number of the agents (∼400 converge step).

INDEX TERMS Holonomic system, decentralized control, nonholonomic agent, formation control, unicycle model.

I. INTRODUCTION

In sub-research fields of decentralized controls, such as consensus theory and formation control, numerous control laws for holonomic systems have been reported [1], [2], [3], [4]. Nevertheless, decentralized control should be applied to nonholonomic systems having constraints in movement, such as vehicles. Notably, several studies have been reported wherein a decentralized control is initially developed for nonholonomic systems, or an algorithm for a holonomic system-based control law is extended by limiting certain conditions [5], [6], [7], [8], [9], [10], [11], [12]. However, existing studies on holonomic systems cannot be directly applied to nonholonomic systems. Therefore, the motivation of this study aims to incorporate control laws targeting holonomic systems into nonholonomic systems.

When implementing holonomic system-based control laws, specially designed robots such as multicopters and omnidirectional-wheeled mobile robots are preferred. Typically, nonholonomic systems are more widely used than holonomic systems, and studies on nonholonomic systems are more practical. Although developing a certain control law by considering nonholonomic systems is more convenient, extending all control laws to various models for nonholonomic systems is time-consuming and inefficient. Therefore, this study develops a strategy that allows nonholonomic systems to use control laws based on holonomic systems. When a nonholonomic system executes a control law targeting

The associate editor coordinating the review of this manuscript and approving it for publication was Qiang Li.

holonomic systems, the system cannot produce the desired output owing to the constraint of the moving direction, causing a phenomenon in which an inappropriate value is fed back. In this situation, by modifying the local frame-dependent variables in the original control law, the nonholonomic system can execute the holonomic-system-based control law without the divergence of the control input.

A. RELATED WORKS

Several studies on decentralized control have been reported [1], [2], [13], [14], [15], [16]. Control laws, when local variables and the shape of formation are given, can be classified into displacement-, distance-, and angle-based controls [1]. When implementing distance-based [17], [18], [19], [20], [21] and angle-based control laws [22], [23], [24], decentralized controllers are not affected by the orientation angle of the local frame. Control laws in which the states of controllers depend on the local frame generally assume that the orientation angle of the local frame is identical to that of the global frame [25]. Moreover, the orientation angles of other agents are compared with those of neighboring agents [26], [27], or the velocity constraints of vehicles are monitored [28]. In studies considering both orientation and nonholonomic constraint simultaneously, methods that periodically change the angular velocity of agents [5] or converge the positions and the orientations of the agents to locally given formation with orientations have been employed [11].

B. CONTRIBUTIONS

In this study, we propose an instant orientation correction strategy (IOCS) satisfying nonholonomic constraints by correcting the reference frame of each agent. Because of nonholonomic constraints, numerous decentralized control approaches are not physically feasible when directly applied to nonholonomic systems. Therefore, the proposed IOCS corrects local variables in a local frame used in a holonomic system-based control law considering the difference in the orientation angles between the local frames of the nonholonomic agent and intermediate state.

II. METHODOLOGY

For a state space vector $\boldsymbol{x} \in \Re^n$, the elements of the vector $\boldsymbol{x}$ are denoted by $x_1, x_2, \cdots, x_n \in \Re$, and the Euclidean norm of $\boldsymbol{x}$ is denoted by $||\boldsymbol{x}||$. For the vectors $\boldsymbol{x}_1, \boldsymbol{x}_2, \cdots, \boldsymbol{x}_n \in \Re^d$, an integrated vector is denoted by $[\boldsymbol{x}_1^{\mathrm{T}}, \cdots, \boldsymbol{x}_n^{\mathrm{T}}]^{\mathrm{T}} \in \Re^{dn\times 1}$. For the angle element θ_i, a counter-clockwise rotation matrix is denoted by $\boldsymbol{R}_{\theta_i} \in \Re^{d\times d}$. For a variable x, the estimation and the time derivative of x are denoted by $\hat{x}$, and $\dot{x}$, respectively.

A. GRAPH THEORY

The basic graph theory is introduced in [29]. Interactive network can be represented using the graph $\mathcal{G} = (\mathcal{V}, \mathcal{E})$, where $\mathcal{V} = 1, 2, \cdots, n$ is the set of n nodes, and $\mathcal{E} \subseteq \mathcal{V} \times \mathcal{V}$ is the edges connecting the nodes. Especially, a set of node js connected to a certain node i through edges are referred to as neighboring nodes $\mathcal{N}_i = \{j \in \mathcal{V} : (i, j) \in \mathcal{E}\}$, where (i, j) is an edge from i to j. In this study, we ignore the case of a self-loop (i, i). The direction of an edge is indicated by an arrow and denotes the state observation between nodes, that is, the node located at the tail of the arrow observes the state of that located at the head. A specific node that does not observe any nodes is represented as a leader node.

The graph $\mathcal{G}$ can represent the adjacency matrix, which includes node and edge information. An adjacency matrix is an $n \times n$ square matrix, and its elements are determined according to the neighboring relationships between nodes. If a graph has no weight at all edges, the elements of the adjacency matrix for the graph are determined as follows:

$$a_{ij} = \begin{cases} 1, & (i,j) \in \mathcal{E}, \\ 0, & \text{else.} \end{cases} \tag{1}$$

A consensus system for a node state x_i, which converges to the average of neighboring node states is expressed as

$$\dot{x}_i = \sum_{j\in\mathcal{N}_i} a_{ij}\left(x_j - x_i\right). \tag{2}$$

For all nodes, (2) can be expressed as

$$\dot{\boldsymbol{x}} = -\boldsymbol{L}\boldsymbol{x}, \tag{3}$$

where $\boldsymbol{x}$ is a state vector $[x_1, x_2, \cdots, x_n]^{\mathrm{T}}$, and $\boldsymbol{L}$ is a Laplacian matrix whose elements are defined as

$$l_{ij} = \begin{cases} -a_{ij}, & (i,j) \in \mathcal{E} \text{ and } i \neq j, \\ \sum_{k\in\mathcal{N}_i} a_{ik}, & i = j, \\ 0, & \text{else.} \end{cases} \tag{4}$$

B. NONHOLONOMIC CONSTRAINT

Constraints are relationships between variables that a system physically obeys. For any system, the configuration space $\mathcal{Q}$, which is the set of all the locations that the system can reach can be defined. This set contains generalized coordinates $q_1, q_2, \cdots, q_n$, which represent the independent variables that can express the system in a minimal number. If the form of a vector constraint $\boldsymbol{q} = [q_1, \cdots, q_n]^{\mathrm{T}} \in \mathcal{Q}$ consisting of generalized coordinates is in the form of (5), a function h_i is termed a holonomic constraint.

$$h_i(\boldsymbol{q}) = 0, \tag{5}$$

where $i = 1, \cdots, k < n$, and k is the number of constraints. Next, (5) can be transformed into (6) by time derivative:

$$\frac{\mathrm{d}}{\mathrm{d}t}h_i(\boldsymbol{q}) = \sum_{j=1}^{n} \frac{\partial h_i}{\partial q_j}\frac{\mathrm{d}q_j}{\mathrm{d}t} = 0. \tag{6}$$

If we define $\boldsymbol{H}_i := \left[\frac{\partial h_i}{\partial q_1}, \cdots, \frac{\partial h_i}{\partial q_n}\right]$, (6) can be simplified by using dot product:

$$\boldsymbol{H}_i \cdot \dot{\mathrm{q}} = 0. \tag{7}$$

Generally, the constraint of a system is described in the form:

$$\boldsymbol{\omega}_i \cdot \dot{\boldsymbol{q}} = 0. \tag{8}$$

If $\boldsymbol{\omega}_i$ can be integrated by all the elements of $\boldsymbol{q}$, that is, $\boldsymbol{\omega}_i$ can be expressed in the form $\boldsymbol{H}_i$, (8) is considered a holonomic constraint. Otherwise, if (8) cannot be integrated in the form (5), it is considered a nonholonomic constraint.

A holonomic system indicates that all the constraints in the system are holonomic, and a system that has at least one nonholonomic constraint is considered a nonholonomic system [30].

C. REFERENCE FRAME

Variables that require geographical criteria must be defined in a specific reference frame. We can define a global reference frame in the form ${}^{\mathrm{g}}\Sigma$, which is the absolute basis for the measurement of variables. Moreover, we classify a specific reference frame that can be defined for each agent i in a local frame in the form ${}^{\ell}\Sigma_i$, where ℓ is the abbreviation of local. The agents are represented by a local frame, that is, the local frame corresponding to each agent has an orientation and origin according to the direction and position of the agent. In particular, we distinguish the local frames for holonomic agents, nonholonomic agents, and intermediate state in the form ${}^{\ell}_{\mathrm{h}}\Sigma$, ${}^{\ell}_{\mathrm{n}}\Sigma$, and ${}^{\ell}_{\mathrm{m}}\Sigma$, respectively. Moreover, a common frame ${}^{\mathrm{c}}\Sigma$ is introduced to compare the variables on each local frame [31]. The common frame has a certain angle to which total agents converge to the specific computed angle determined by the graph node edges and initial angles of each agent as its orientation angle.

For variables, a left superscript, left subscript, right superscript, and right subscript are used as the characteristics of the frame, the characteristics of the agent, the agent as an observation reference, and the agent to which the variable belongs, respectively. Particularly, the explanation of the agent is included in the right subscript and separated by a comma. For example, ${}^{\ell}_{\mathrm{h}}\boldsymbol{p}^i_j$ is a relative variable $\boldsymbol{p}$ of an agent j observed in the *local* ${}^{\mathrm{h}}\Sigma$ of an agent i.

D. ORIENTATION ALIGNMENT-BASED FORMATION CONTROL

An OAFC is a decentralized formation control based on orientation alignment and position estimation [27].

$$ {}^{\mathrm{g}}_{\mathrm{h}}\dot{\theta}_i = -k_\theta \sum_{j\in\mathcal{N}_i} a_{ij} \left({}^{\mathrm{g}}_{\mathrm{h}}\theta_j - {}^{\mathrm{g}}_{\mathrm{h}}\theta_i\right), \tag{9} $$

$$ {}^{\mathrm{c}}\dot{\hat{\boldsymbol{p}}}_i = -k_{\hat{p}} \sum_{j\in\mathcal{N}_i} a_{ij} \left[\left({}^{\mathrm{c}}\hat{\boldsymbol{p}}_j - {}^{\mathrm{c}}\hat{\boldsymbol{p}}_i\right) - \left({}_{\mathrm{h}}\boldsymbol{p}^i_j - {}_{\mathrm{h}}\boldsymbol{p}^i_i\right)\right] + {}_{\mathrm{h}}\boldsymbol{v}^i_i, \tag{10} $$

$$ {}_{\mathrm{h}}\boldsymbol{v}^i_i = -k_p \left({}^{\mathrm{c}}\boldsymbol{p}_{i,*} - {}^{\mathrm{c}}\hat{\boldsymbol{p}}_i\right), \tag{11} $$

where k_θ, $k_{\hat{p}}$, and k_p are the proper gains, θ_i is the orientation angle of an agent i with respect to ${}^{\mathrm{g}}\Sigma$, $\boldsymbol{p}^i_j$ is the relative position of an agent j from an agent i, ${}^{\mathrm{c}}\hat{\boldsymbol{p}}_i$ is the estimated position of an agent i in ${}^{\mathrm{c}}\Sigma$, and ${}^{\mathrm{c}}\boldsymbol{p}_{i,*}$ is the final desired position of an agent i.

An orientation alignment (9) converges the orientations of agents to a consensus angle corresponding to the topology of the graph $\mathcal{G}$ over time. In this case, the converged angle functions as a common orientation for all the agents, allowing the comparison of their relative positions. Therefore, the frame with the angle as the orientation is set as ${}^{\mathrm{c}}\Sigma$. A position estimation (10) estimates the position of the agent $\hat{\boldsymbol{p}}^{\mathrm{c}}_i$ based on the relative positions within ${}^{\mathrm{c}}\Sigma$. A formation control (11) moves the agent so that the estimated position ${}^{\mathrm{c}}\hat{\boldsymbol{p}}_i$ in ${}^{\mathrm{c}}\Sigma$ is the same as the desired position ${}^{\mathrm{c}}\boldsymbol{p}_{i,*}$.

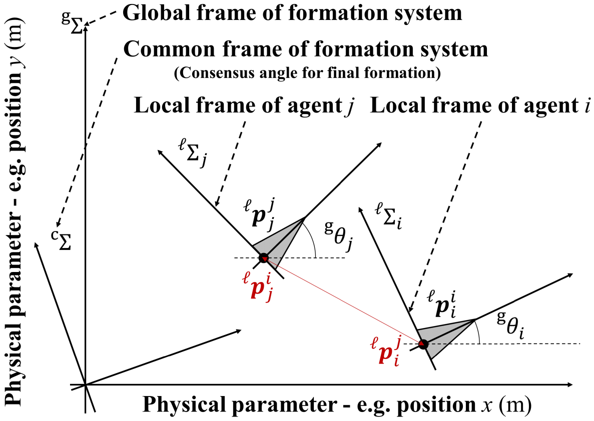
${}^{\mathrm{g}}\Sigma$
Global frame of formation system
Common frame of formation system
(Consensus angle for final formation)
Local frame of agent j
Local frame of agent i
${}^{\ell}\Sigma_j$
${}^{\ell}\boldsymbol{p}^j_j$
${}^{\mathrm{g}}\theta_j$
${}^{\ell}\Sigma_i$
${}^{\mathrm{c}}\Sigma$
${}^{\ell}\boldsymbol{p}^i_j$
${}^{\ell}\boldsymbol{p}^i_i$
${}^{\mathrm{g}}\theta_i$
${}^{\ell}\boldsymbol{p}^j_i$
Physical parameter - e.g. position y (m)
Physical parameter - e.g. position x (m)

FIGURE 1. Reference frames and variables of agents, where ${}^{\ell}_{\mathrm{h}}p^i_j$ is a relative position vector p of certain agent j observed from reference frame of ${}^{\ell}\Sigma$ regarding the agent i. In addition, θ represents the orientation angles of each agent. It should be noted that the common frame ${}^{\mathrm{c}}\Sigma$ is the consensus frame in which total agents converge to the specific computed value determined by the graph node edges and initial angles of each agent.

E. INSTANT ORIENTATION CORRECTION STRATEGY

Due to the nonholonomic constraints, direct implementation of orientation alignment control for the holonomic systems is not applicable to the nonholonomic systems. The core concept of IOCS is to follow the virtual desired positions of agents to eventually follow the local desired positions of the agents.

Fig. 2 shows the entire system including the holonomic system-based control law (HSCL), the nonholonomic control stage (NCS), and the IOC). An HSCL is an equation in which the positional variables of OAFC for nonholonomic systems are replaced with the corrected values of IOCS.

$$ {}_{\mathrm{m}}\dot{\theta}_i = -k_\theta \sum_{j\in\mathcal{N}_i} a_{ij} \left({}^{\mathrm{g}}_{\mathrm{n}}\theta_j - {}^{\mathrm{g}}_{\mathrm{n}}\theta_i\right), \tag{12} $$

$$ \begin{aligned} {}^{\mathrm{c}}\dot{\hat{\boldsymbol{p}}}_i = -k_{\hat{p}} \sum_{j\in\mathcal{N}_i} a_{ij} \left[\left({}^{\mathrm{c}}\hat{\boldsymbol{p}}_j - {}^{\mathrm{c}}\hat{\boldsymbol{p}}_i\right) - \boldsymbol{R}^{-1}_{\psi_i}\left({}_{\mathrm{m}}\boldsymbol{p}^i_j - {}_{\mathrm{m}}\boldsymbol{p}^i_i\right)\right] \\ + \boldsymbol{R}^{-1}_{\psi_i}\ {}_{\mathrm{m}}\boldsymbol{v}^i_i, \end{aligned} \tag{13} $$

$$ {}_{\mathrm{m}}\boldsymbol{v}^i_i = -k_p \boldsymbol{R}_{\psi_i} \left({}^{\mathrm{c}}\boldsymbol{p}_{i,*} - {}^{\mathrm{c}}\hat{\boldsymbol{p}}_i,\right), \tag{14} $$

$$ {}^{\mathrm{g}}_{\mathrm{n}}\theta_i = \mathcal{W}\left({}^{\mathrm{g}}_{\mathrm{m}}\theta_i\right), \tag{15} $$

where ${}^{\mathrm{g}}_{\mathrm{n}}\theta_i$ is the orientation angle of a nonholonomic agent i, ${}^{\mathrm{g}}_{\mathrm{m}}\theta_i$ is the intermediate angle of a nonholonomic agent i, ${}_{\mathrm{m}}\boldsymbol{p}^i_i$ is the intermediate position of a nonholonomic agent i,

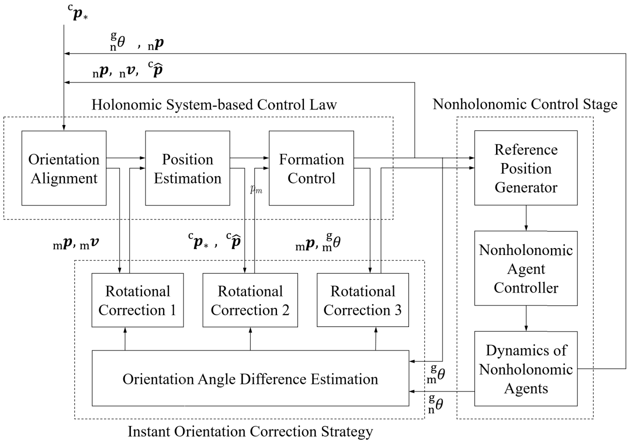
${}^{\mathrm{c}}\boldsymbol{p}_*$
${}^{\mathrm{g}}_{\mathrm{n}}\theta$, ${}_{\mathrm{n}}\boldsymbol{p}$
${}_{\mathrm{n}}\boldsymbol{p}$, ${}_{\mathrm{n}}\boldsymbol{v}$, ${}^{\mathrm{c}}\hat{\boldsymbol{p}}$
Holonomic System-based Control Law
Nonholonomic Control Stage
Orientation Alignment
Position Estimation
Formation Control
p_m
Reference Position Generator
Nonholonomic Agent Controller
Dynamics of Nonholonomic Agents
${}_{\mathrm{m}}\boldsymbol{p}$, ${}_{\mathrm{m}}\boldsymbol{v}$
${}^{\mathrm{c}}\boldsymbol{p}_*$, ${}^{\mathrm{c}}\hat{\boldsymbol{p}}$
${}_{\mathrm{m}}\boldsymbol{p}$, ${}^{\mathrm{g}}_{\mathrm{m}}\theta$
Rotational Correction 1
Rotational Correction 2
Rotational Correction 3
Orientation Angle Difference Estimation
${}^{\mathrm{g}}_{\mathrm{m}}\theta$
${}^{\mathrm{g}}_{\mathrm{n}}\theta$
Instant Orientation Correction Strategy

FIGURE 2. The block diagram of formation control system including instant orientation correction strategy. First the holonomic system-based control is processed based on the position vector p, velocity vector v, and orientation angle θ of each agents. Next, instant orientation correction process is carried out during orientation alignment, position estimation, and formation control. Finally, nonholonomic control is applied to generate reference positions.

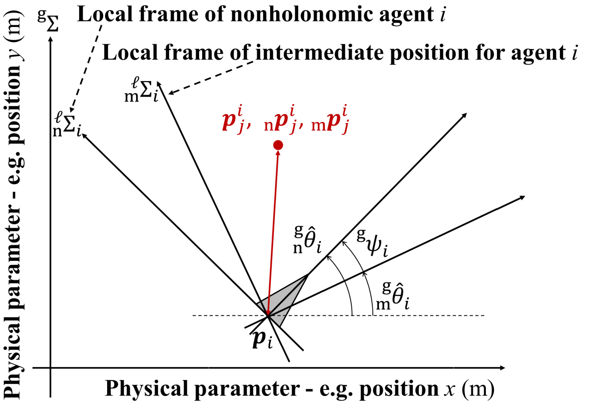
${}^{\mathrm{g}}\Sigma$
Local frame of nonholonomic agent i
Local frame of intermediate position for agent i
${}^{\ell}_{\mathrm{m}}\Sigma_i$
${}^{\ell}_{\mathrm{n}}\Sigma_i$
$\boldsymbol{p}^i_j$, ${}_{\mathrm{n}}\boldsymbol{p}^i_j$, ${}_{\mathrm{m}}\boldsymbol{p}^i_j$
${}^{\mathrm{g}}_{\mathrm{n}}\hat{\theta}_i$
${}^{\mathrm{g}}\psi_i$
${}^{\mathrm{g}}_{\mathrm{m}}\hat{\theta}_i$
$\boldsymbol{p}_i$
Physical parameter - e.g. position y (m)
Physical parameter - e.g. position x (m)

FIGURE 3. Instant orientation correction strategy (IOCS) and local frames of nonholonomic ${}^{\ell}_{\mathrm{n}}\Sigma_i$ and intermediate position ${}^{\ell}_{\mathrm{m}}\Sigma_i$ for agent i. Here, ψ is a converging angle which denotes the difference between ${}^{\mathrm{g}}_{\mathrm{m}}\theta$ and ${}^{\mathrm{g}}_{\mathrm{n}}\theta$. Due to the nonholonomic constraint, IOCS handles ψ to converge for the desired position and orientation angle of each of the agents.

and $\mathcal{W}(x)$ is a certain function that follows connectivity between ${}^{\ell}_{\mathrm{m}}\Sigma$ and ${}^{\ell}_{\mathrm{n}}\Sigma$ generated by nonholonomic constraints.

The IOCS rotates variables in ${}^{\ell}_{\mathrm{m}}\Sigma$ and ${}^{\mathrm{c}}\Sigma$ by $\boldsymbol{R}_{\psi_i}$ with respect to their origin. The rotation angles for correction are calculated using (17), and the calculation is based on the estimated orientation of ${}^{\ell}_{\mathrm{h}}\Sigma$. The corrected control target values in (19) are used as control inputs of nonholonomic agents. Notably, a nonholonomic agent cannot perfectly reflect an intermediate state as its physical motion because of its nonholonomic constraints. Therefore, the intermediate angles and positions are pursued by nonholonomic agents, as the local target orientation angles and positions. This property is represented by the local target position in (19).

$$
\begin{aligned}
{}_{\mathrm{h}}\dot{\hat{\boldsymbol{\theta}}} &= -k_{\psi}\boldsymbol{L}\left({}_{\mathrm{h}}\hat{\boldsymbol{\theta}} - {}^{\mathrm{g}}_{\mathrm{m}}\boldsymbol{\theta} - \boldsymbol{\psi}\right), && (16)\\
\dot{\boldsymbol{\psi}} &= -k_{\psi}\boldsymbol{L}\left({}_{\mathrm{h}}\hat{\boldsymbol{\theta}} - {}^{\mathrm{g}}_{\mathrm{n}}\boldsymbol{\theta}\right), && (17)\\
{}_{\mathrm{n}}\boldsymbol{p}^i_{i,*} &= \boldsymbol{R}^{-1}_{\psi_i}\ {}_{\mathrm{m}}\boldsymbol{p}^i_i, && (18)\\
{}^{\mathrm{g}}_{\mathrm{n}}\theta_{i,*} &= {}^{\mathrm{g}}_{\mathrm{m}}\theta_i - \psi_i, && (19)
\end{aligned}
$$

where ${}_{\mathrm{h}}\hat{\boldsymbol{\theta}}$ is the estimated orientation angles of virtual holonomic agents, $\boldsymbol{\psi}$ is the converging angle to the orientation angle difference between ${}^{\mathrm{g}}_{\mathrm{m}}\boldsymbol{\theta}$ and ${}^{\mathrm{g}}_{\mathrm{n}}\boldsymbol{\theta}$, and ${}_{\mathrm{n}}\boldsymbol{p}^i_{i,*}$ is the local target position in ${}^{\ell}_{\mathrm{n}}\Sigma_i$ seen from an agent i.

The major challenge arises from the difference between the orientations of ${}^{\ell}_{\mathrm{n}}\Sigma$ and ${}^{\ell}_{\mathrm{m}}\Sigma$. The mismatch of the orientation occurs because of the disturbance, dynamic model, and controller of nonholonomic systems. If a nonholonomic agent follows (9), we must consider the function $\mathcal{W}(x)$ that represents the aforementioned mismatch effect. ${}^{\mathrm{g}}_{\mathrm{m}}\boldsymbol{\theta}$, which does not match the actual movement of nonholonomic agents, is used as the target angular velocity. Therefore, the orientation angles of nonholonomic agents diverge. Owing to an abnormality in ${}^{\ell}_{\mathrm{n}}\Sigma$, the relative position to other nonholonomic agents also diverges.

The IOCS corrects the difference in the orientations between ${}^{\ell}_{\mathrm{n}}\Sigma$ and ${}^{\ell}_{\mathrm{m}}\Sigma$. Because ${}^{\mathrm{g}}_{\mathrm{m}}\boldsymbol{\theta}$ is used as the desired orientation angle of the nonholonomic agent, the control of the agent should be performed according to ${}^{\ell}_{\mathrm{m}}\Sigma$. Therefore, for the local variables of ${}^{\ell}_{\mathrm{h}}\Sigma$ and ${}^{\ell}_{\mathrm{m}}\Sigma$ to have the same value, a correction is required to rotate the local variables of ${}^{\ell}_{\mathrm{n}}\Sigma$ by an angle difference between the orientation angles of ${}^{\ell}_{\mathrm{n}}\Sigma$ and ${}^{\ell}_{\mathrm{m}}\Sigma$. The orientation angle difference is estimated in (17) and $\boldsymbol{\psi}$. In (13) and (14), the rotation matrix $\boldsymbol{R}_{\psi_i}$ is applied to the relative position of an agent j with respect to the origin of an agent i. Through this process, $\boldsymbol{\psi}$ converges to ${}^{\mathrm{g}}_{\mathrm{n}}\boldsymbol{\theta} - {}^{\mathrm{g}}_{\mathrm{m}}\boldsymbol{\theta}$. Therefore, the relative positions in ${}^{\ell}_{\mathrm{m}}\Sigma$ are rotated by $+\boldsymbol{\psi}$ from the orientation of ${}^{\ell}_{\mathrm{n}}\Sigma$, and the relationship between the relative positions of an agent j observed in ${}^{\ell}_{\mathrm{n}}\Sigma$ and ${}^{\ell}_{\mathrm{m}}\Sigma$ is expressed as

$$
{}_{\mathrm{n}}\boldsymbol{p}^i_j = \boldsymbol{R}^{-1}_{\psi_i}\ {}_{\mathrm{m}}\boldsymbol{p}^i_j. \qquad (20)
$$

For (14), the local variables in ${}^{\ell}_{\mathrm{m}}\Sigma$ exist on the left-hand side. Therefore, the correction is achieved by rotating the variables in ${}^{\mathrm{c}}\Sigma$ on the right-hand side by $+\boldsymbol{\psi}$, instead. Fig. 3 shows the correction process of the IOCS through the values of the local variables in ${}^{\ell}_{\mathrm{n}}\Sigma$ and ${}^{\ell}_{\mathrm{m}}\Sigma$.

The intermediate state calculated using (14) is input to the NCS as the local target for each agent. Because the frames to which the local target and nonholonomic agent belong are different, ${}^{\ell}_{\mathrm{m}}\Sigma$ is converted into ${}^{\ell}_{\mathrm{n}}\Sigma$ using (20).

Correction algorithms have complexities for the dimension d and number of agents n. The local variable correction of an HSCL has a complexity of $\mathcal{O}(d^2)$ because it is a rotational transformation for a dimension. The IOCS for estimating the required rotation angle $\boldsymbol{\psi}$ has a complexity of $\mathcal{O}(n^2)$. The HSCL expression has a complexity of $\mathcal{O}(n^2d^2)$.

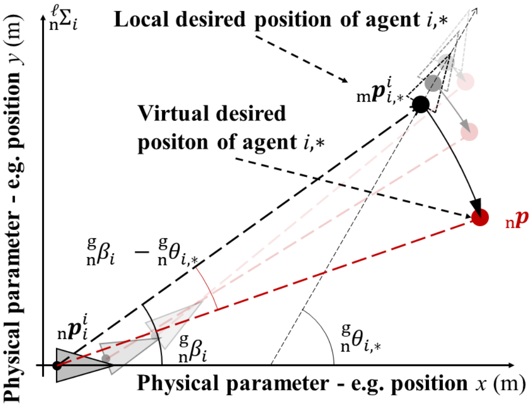
${}^{\ell}_{\mathrm{n}}\Sigma_i$
Local desired position of agent $i,*$
${}_{\mathrm{m}}\boldsymbol{p}^i_{i,*}$
Virtual desired positon of agent $i,*$
${}_{\mathrm{n}}\boldsymbol{p}^i_{i,\star}$
${}^{\mathrm{g}}_{\mathrm{n}}\beta_i - {}^{\mathrm{g}}_{\mathrm{n}}\theta_{i,*}$
${}_{\mathrm{n}}\boldsymbol{p}^i_i$
${}^{\mathrm{g}}_{\mathrm{n}}\beta_i$
${}^{\mathrm{g}}_{\mathrm{n}}\theta_{i,*}$
Physical parameter - e.g. position y (m)
Physical parameter - e.g. position x (m)

FIGURE 4. The geometric relation between the local desired position ${}_{\mathrm{n}}p^i_{i,*}$ and the virtual desired position ${}_{\mathrm{n}}p^i_{i,\star}$. The virtual desired position is generated position by reference position generator from the local desired position by the angle of ${}^{\mathrm{g}}_{\mathrm{n}}\beta_i - {}^{\mathrm{g}}_{\mathrm{n}}\theta_{i,*}$ where ${}^{\mathrm{g}}_{\mathrm{n}}\beta_i$ is the angle of the local desired position seen from ${}^{\ell}_{\mathrm{n}}\Sigma_i$, and ${}^{\mathrm{g}}_{\mathrm{n}}\theta_{i,*}$ is the local desired angle of the agent i. It should be noted that the transparent points represent each sequentially changing virtual and local desired positions.

F. APPLICATION TO NONHOLONOMIC AGENTS

A nonholonomic agent must converge to the desired orientation while executing point-to-point motion. One such algorithm proposed in [32] generates a reference position according to the following equation:

$$\begin{aligned} {}_{\mathrm{n}}\boldsymbol{p}^i_{i,\star} &= \boldsymbol{R}_{{}^{\mathrm{g}}_{\mathrm{n}}\beta_i - {}^{\mathrm{g}}_{\mathrm{n}}\theta_{i,*}}\, {}_{\mathrm{n}}\boldsymbol{p}^i_{i,*}, \\ {}^{\mathrm{g}}_{\mathrm{n}}\beta_i &= \tan^{-1}\left(\frac{{}_{\mathrm{n}}p^i_{i,y,*}}{{}_{\mathrm{n}}p^i_{i,x,*}}\right) + {}^{\mathrm{g}}_{\mathrm{n}}\theta_i, \end{aligned} \tag{21}$$

where ${}_{\mathrm{n}}\boldsymbol{p}^i_{i,\star}$ is a virtual desired position, as a new local desired position, of a nonholonomic agent i, ${}^{\mathrm{g}}_{\mathrm{n}}\theta_{i,*}$ is the corrected desired angle, and ${}_{\mathrm{n}}\boldsymbol{p}^i_{i,*}$ is the corrected intermediate position, as an old local desired position, of the nonholonomic agent i. The nonholonomic agent moves to the virtual desired position ${}_{\mathrm{n}}\boldsymbol{p}^i_{i,\star}$ instead of the original local desired position ${}_{\mathrm{n}}\boldsymbol{p}^i_{i,*}$. Fig. 4 shows the geometric relationship between the variables in ${}^{\ell}_{\mathrm{n}}\Sigma$.

However, this algorithm cannot achieve the orientation alignment for a moving target position. In this study, as the positions of agents gradually converge to a certain value over time, this corresponds to a case in which the target position moves. When the target position moves, the virtual desired position moves accordingly, and the nonholonomic agent moves toward the virtual desired position. At this time, as the virtual desired position continues to move in a direction independent of the target orientation angle, the orientation of the nonholonomic agent moving to the virtual desired position is also aligned with that of the moving vector of the virtual desired position. To address this challenge, an update step size λ was introduced. The virtual desired position is updated to a new target whenever the distance between the old virtual desired position and the updated virtual desired position is more than a tolerance λ. Otherwise, the old virtual desired position does not update to a new target.

G. UNICYCLE-MODELED AGENT CONTROL

The linear and angular velocities of the unicycle-modeled nonholonomic agent are calculated using the position, orientation, and target position as follows:

$$\begin{aligned} {}_{\mathrm{n}}v^i_i &= k_v \|{}_{\mathrm{n}}\boldsymbol{p}^i_{i,\star}\| \cos({}^{\mathrm{g}}_{\mathrm{n}}\beta_i), \\ {}_{\mathrm{n}}\omega^i_i &= k_\omega \sin({}^{\mathrm{g}}_{\mathrm{n}}\beta_i), \end{aligned} \tag{22}$$

where k_v and k_ω are positive constants. For convenience, the velocities of the nonholonomic agent were defined as (22).

III. EXPERIMENTAL SETUP

In this section, general experimental conditions and the various apparatus are explained.

A. SIMULATION: COMPARISON OF HSCL WITH AND WITHOUT IOCS

The simulations were performed for 300 iterations each, and the initial positions and angles of the agents were randomly arranged for each simulation. Moreover, the simulation conditions including the initial positions, target positions, and simulation time were set equally for the condition with and without the IOCS. The desired positions for nonholonomic agents were (320, 360), (200, 240), (320, 120), and (440, 240) pixels.

B. SIMULATION: IOCS UNDER A DYNAMIC SCENARIO

A simulation was performed for the condition that the desired position changes. During the simulation, desired positions were converted to another position at 300 iteration times. The initial positions and angles of the agents were randomly arranged for each simulation. The initial desired positions were (240, 160), (400, 160), (240, 320), and (400, 320) pixels. The final desired positions were (320, 360), (400, 80), (80, 400), and (400, 400) pixels.

C. EXPERIMENT: AGENT CONTROL SYSTEM

As shown in Fig 5, four unicycle-modeled E-pucks were used as nonholonomic system agents (GCtronic, Swiss). The initial position of the nonholonomic agents x and y were given randomly within the range of ±3 m, respectively. Additionally, the orientation angles of the agents were given randomly within the range of $\pm\pi$ rad. Particularly, the orientation of the leading agent was aligned to that of ${}^{\mathrm{g}}\Sigma$. Therefore, the consensus angle $\boldsymbol{\theta}_*$ at which the agents finally converge is 0 rad. The positions and orientations of nonholonomic agents were measured by the OpenCV-based object detection algorithm using a web camera that has a maximum video resolution of 4096 × 2160 pixels and a maximum frame rate of 90 fps (Logitech BRIO, Swiss) [33]. However, to prevent computational delay, object detection is performed at a resolution of 640 × 480 pixels and a frame rate of 30 fps. In addition, four distinctive graphical markers were placed on the surface of each of the agents to measure the positions and orientations of each agent. After obtaining the positions and orientation

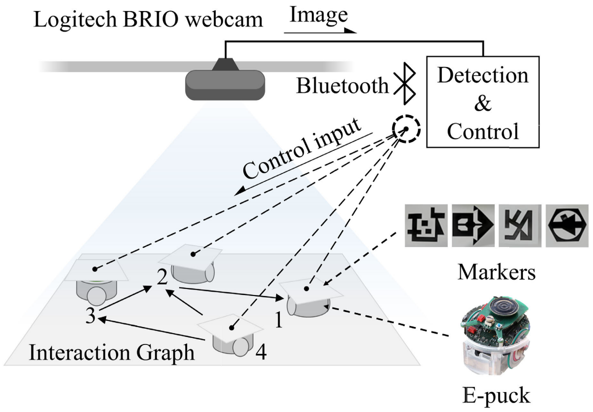

FIGURE 5. The experiments were conducted using a webcam and mobile robots. Field images for nonholonomic agents are recorded by a top-view camera and transmitted to a computing unit. The computing unit receives images from the camera, detects the agents with characteristic markers through an object detection algorithm from OpenCV, and controls each agent via Bluetooth communication. Connections between agents are represented by an interaction graph.

angles of the agents, the control input was transmitted via a Bluetooth protocol.

Image processing and feature detection are performed using oriented FAST and rotated BRIEF (ORB) with OpenCV, and K-means clustering was used to estimate the mean position of the marker detected by the camera [34]. In addition, the direction of the object was determined by calculating the intensity centroid for rotated feature detection using a BRIEF algorithm [35]. Key points and descriptors to distinguish each marker were extracted using ORB from the marker, and the image obtained from the camera were compared with each other. Then, the best-matched section of the image was considered as the position of the agents.

D. SIMULATION: THE UPDATE STEP SIZE EFFICIENCY

A simulation was performed to analyze the convergence efficiency of each agent according to the update step size λ and the number of agents. In each simulation, the cumulative angular differences of all the agents during the simulation between different λs were recorded for eight cases, namely $\lambda = 0.25,\ 0.5,\ 0.75,\ 1.0,\ 1.25,\ 1.5,\ 1.75,$ and 2.0 (pixels). Therefore, a cumulative mean angular velocity error (CMAE) was introduced to evaluate the effect of λ:

$$\mathrm{CMAE} = \frac{1}{N}\sum_{i=1}^{N}\sum_{j=1}^{L}\left|\frac{\left({}_{\mathrm{n}}\theta_{i|j}(\lambda = 0.25) - {}_{\mathrm{n}}\theta_{i|j}(\lambda \neq 0.25)\right)}{t_j}\right|, \tag{23}$$

where L is the number of simulation rounds, N is the number of agents, ${}_{\mathrm{n}}\theta_{i|j}(\lambda = 0.25)$ is the angle record of nonholonomic agents when λ is zero, ${}_{\mathrm{n}}\theta_{i|j}(\lambda \neq 0.25)$ is the angle record of nonholonomic agents for eight cases in which λ is not 0.25, and t_j is the converging time of the agents for each round. Additionally, the CMAE is calculated for four cases according to the number of agents, namely 3, 4, 5, and 6.

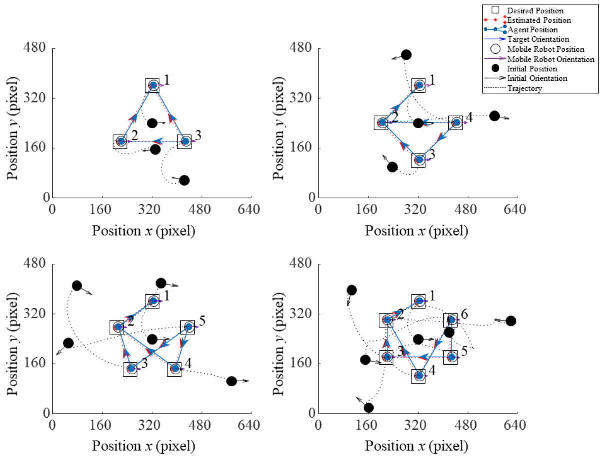

FIGURE 6. Simulation settings and results for each number of agents: 3, 4, 5, and 6. All rounds of simulations were conducted under equal desired positions, target orientations, and interaction graphs. Also, simulations with different lambdas for each simulation rounds have the same initial position so that the comparison can be performed properly.

TABLE 1. IOCS parameters used in the experiment, where b is the distance between the wheels of the E-puck, and k_θ, $k_{\hat{p}}$, k_p, k_v, k_ω are the gains for orientation angle, estimated postion, target velocity, velocity control, angular velocity control respectively.

IOCS Parameter	Value
b (mm)	22
k_θ	5
$k_{\hat{p}}$	5
k_p	4
k_v	4
k_ω	25

To compare the difference according to λs, all the other conditions such as initial positions or initial angles other than λ are the same. The simulation is performed for 1000 rounds ($L = 1000$), and both the initial positions and angles of the agents are randomly arranged for each simulation. In addition, the simulation time step δt was set at 0.02 s with a constant velocity model. Furthermore, the simulation is performed until all the agents are placed in the desired positions. The desired positions are arranged at equal intervals so that the positions forms a circle centered at (320,240) pixels with a radius of 120 pixels, that is, (320, 360), (200, 240), (320, 120), and (440, 240) pixels for four agents. The desired positions, target orientations, and interaction graphs for each number of agents are shown Fig 6.

IV. RESULTS

In this section, the experiment results described in section III are presented. Notably, the IOCS parameters are empirically chosen to control each agent (Table 1).

A. SIMULATION: WITH AND WITHOUT IOCS

Fig. 7 and 8 show the visualized the formation and position errors for each nonholonomic agents under holonomic system-based control without proposed IOCS approach.

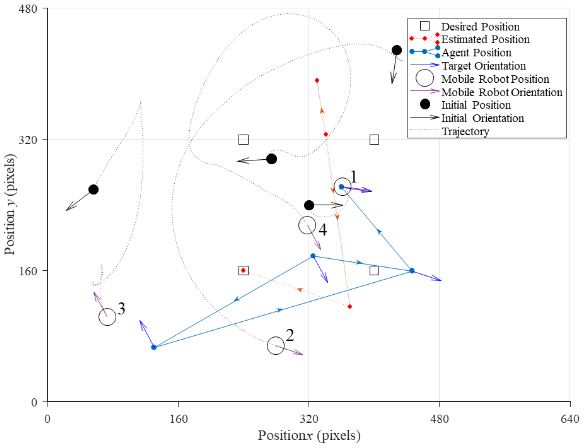

FIGURE 7. The formation result of the HSCL simulation after 300 iterations for the case without IOCS.

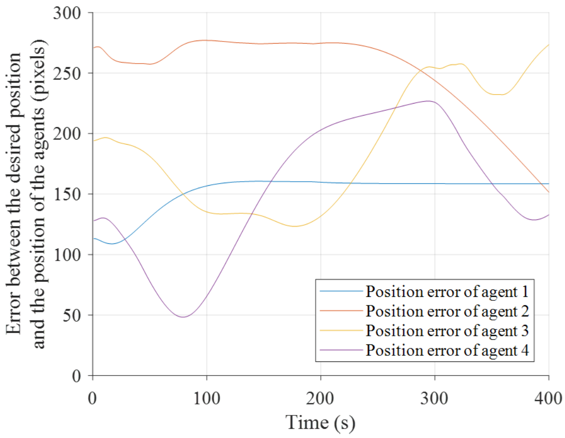

FIGURE 8. The position error of the HSCL simulation after 300 iterations for the case without IOCS.

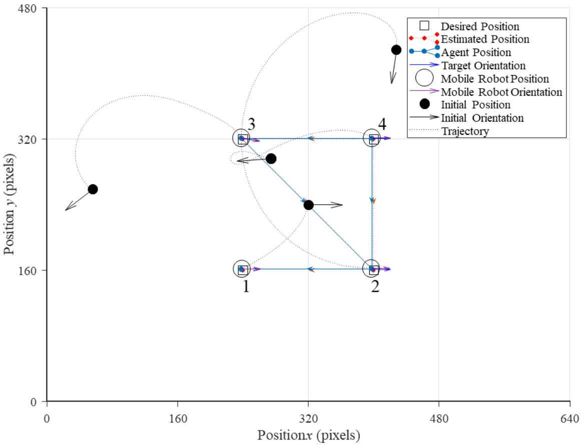

FIGURE 9. The formation result of the HSCL simulation after 300 iterations for the case with IOCS.

Fig. 9 and 10 show the visualized the formation and position errors for each nonholonomic agents under holonomic system-based control with proposed IOCS approach.

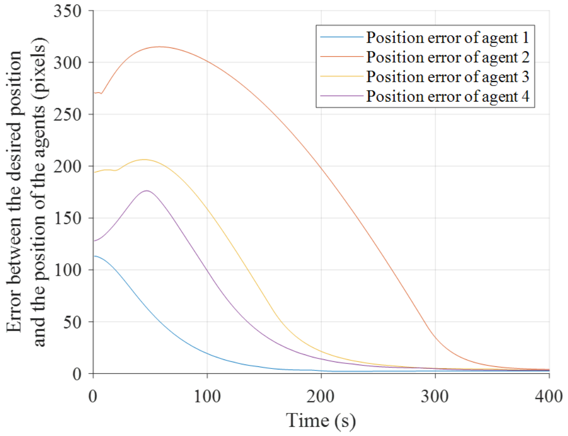

FIGURE 10. The position error of the HSCL simulation after 300 iterations for the case with IOCS.

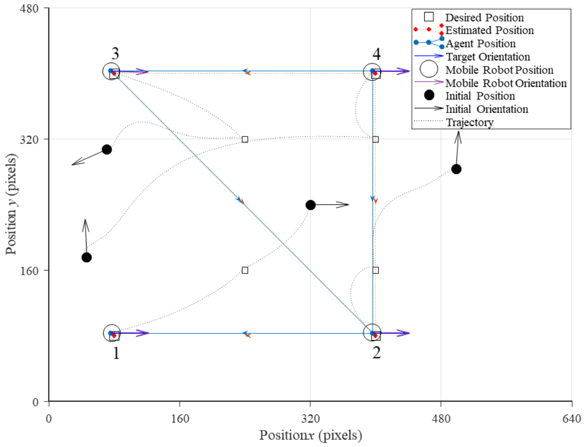

FIGURE 11. The formation result of the simulation under a dynamic scenario. The initial desired position was changed once to the final desired position.

B. SIMULATION: IOCS UNDER A DYNAMIC SCENARIO

Fig. 11 and 12 show the visualized the formation and position errors for each nonholonomic agent under a dynamic scenario in which the initial desired position was switched to another position. The formation control was carried out until all of the agents were located in the final desired position area (12 × 12 pixels).

C. EXPERIMENTAL RESULTS: POSITIONAL RESULT USING THE INSTANT ORIENTATION CORRECTION STRATEGY

Fig 13 shows the initial formation and the final formation of agents during the experiment. The formation control was carried out until all of the agents were located in the desired position area (12 × 12 pixels).

Fig 14 and Fig 15 shows an overall measured positions and intermediate positions of each agents during the agent control experiment using IOCS.

Fig 16 shows absolute error between the desired positions and the positions of the agents.

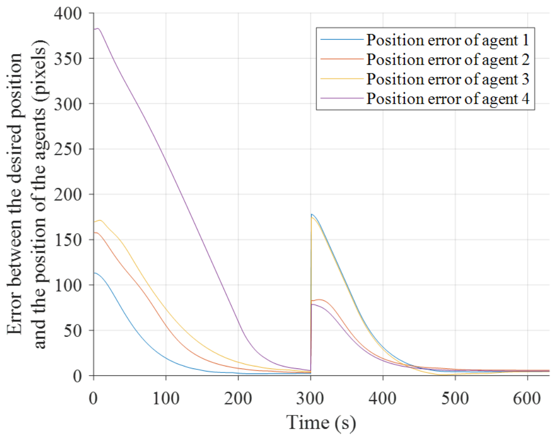

FIGURE 12. The position error of the simulation under a dynamic scenario. The initial desired position changed to the final desired position after 300 iterations from the start of the simulation.

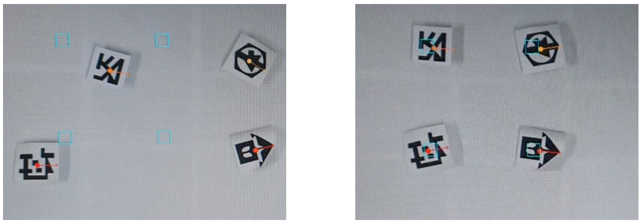

(a) Initial formation.

(b) Final formation.

FIGURE 13. The initial formation and the final formation of nonholonomic agents. Agents were controlled until all of the agents were located in the desired position area.

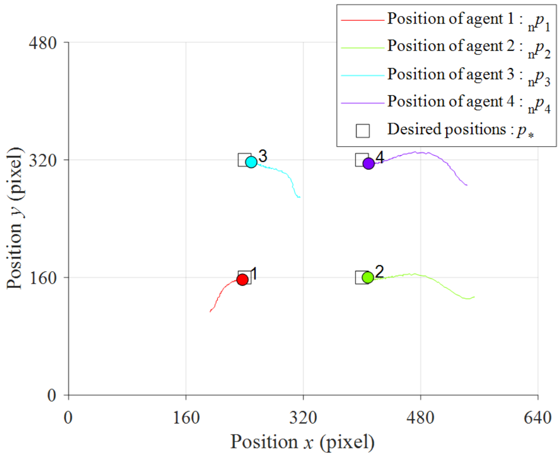

FIGURE 14. Measured positions of agents by the camera when proposed IOCS is applied. The agents were controlled until all of the agents are located in the desired position area (12 × 12 pixels).

D. EXPERIMENTAL RESULTS: ORIENTATION RESULT USING THE INSTANT ORIENTATION CORRECTION STRATEGY

Fig 17 shows a measured orientation angle during the experiment until the agents aligned to the desired angle $\boldsymbol{\theta}_*$.

Fig 18 shows orientation angle difference between the intermediate frame ${}^{\ell}_{m}\Sigma$ and nonholonomic frame ${}^{\ell}_{n}\Sigma$.

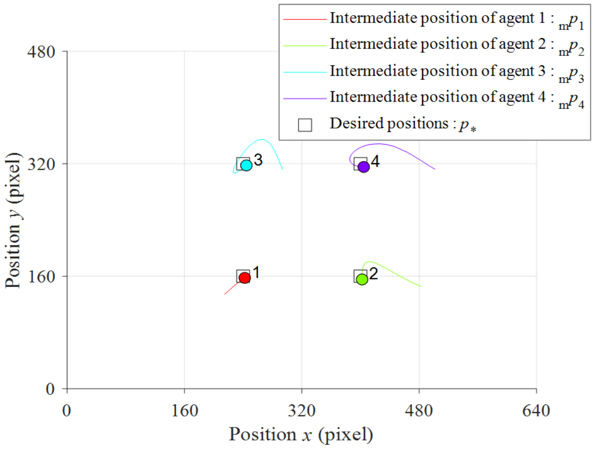

FIGURE 15. Intermediate positions of agents when proposed IOCS is applied. Due to the nonholonomic constraint and the control stage, intermediate position was calculated to follow the local desired positions of agents.

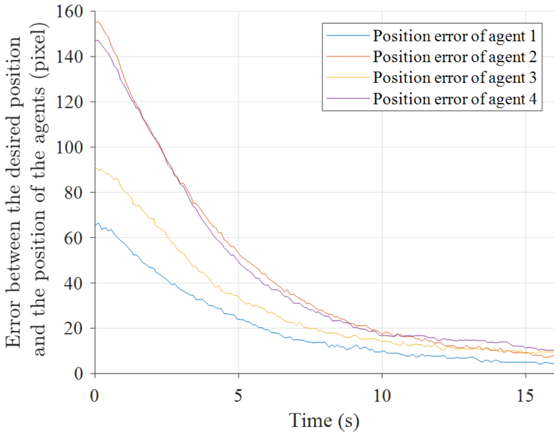

FIGURE 16. Absolute error between the desired positions and the positions of the agents.

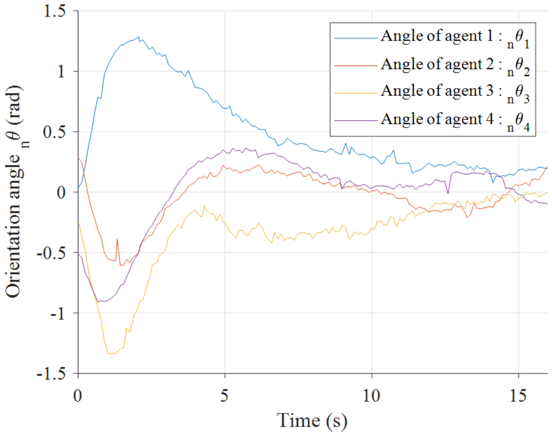

FIGURE 17. Measured orientation angle during the experiment where ${}_{n}\theta$ is the measured orientation angle of the agents. Note that the consensus angle θ_* is set as 0 rad.

Fig 19 shows absolute error between the orientation angle of the common frame ${}^{c}\Sigma$ and the nonholonomic frame ${}^{\ell}_{n}\Sigma$.

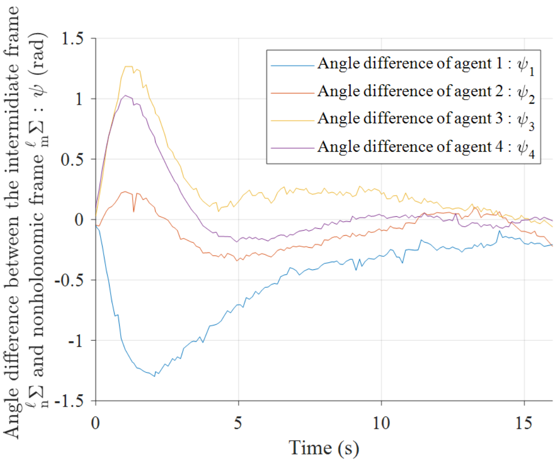

FIGURE 18. Angle difference ψ between the intermediate frame and nonholonomic frame, where ${}^{\ell}_{m}\Sigma$ is the intermediate frame, ${}^{\ell}_{n}\Sigma$ is the nonholonomic frame.

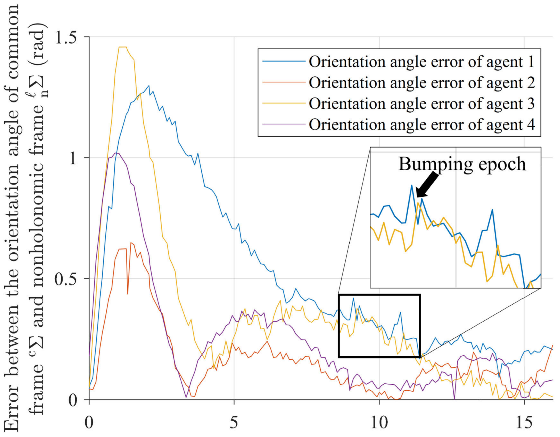

FIGURE 19. Absolute error between the orientation angle of common frame and the nonholonomic frame, where ${}^{c}\Sigma$ is the common frame, and ${}^{\ell}_{n}\Sigma$ is the nonholonomic frame.

E. SIMULATION: λ AND CONVERGE TIME ANALYSIS

Fig 20 shows cumulative mean angular velocity errors (CMAE) according to each value of λ (pixels).

Fig 21 shows required converge step according to each values of λ (pixels).

V. DISCUSSION

In this section, the considerations of the experiment and the simulation results in section IV are discussed.

A. INFLUENCE OF IOCS ON HSCL

The effect of the IOCS can be confirmed through simulations for nonholonomic agents. During the iterations, nonholonomic agents without the IOCS do not make formation, and intermediate positions do not converge to estimate the positions (Fig. 7 and 8). Conversely, as expected, nonholonomic agents with the IOCS are arranged to the desired positions after 300 iterations (Fig. 9 and 10). Furthermore, the effect of IOCS can be confirmed even in the case where the formation dynamically changes (Fig. 11, and 12). Therefore, introducing a frame correction strategy such as the proposed IOCS when implementing holonomic control laws for agents that have nonholonomic constraints is effective.

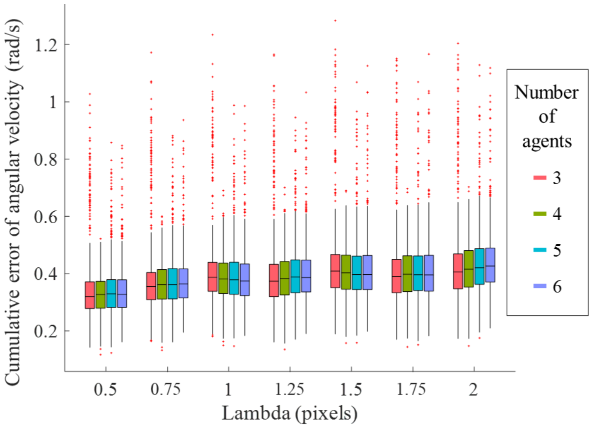

FIGURE 20. Cumulative mean angular velocity errors (CMAE) for each number of agents according to each of the λ for round $L = 1000$. The boxed area represents 50% of the quantile of the cumulative error of angular velocity and red dots denote outlier samples beyond the box area. It can be known that as the λ grows, the cumulative error of angular velocity gets bigger. Note that the error was computed based on the simulation result when λ was 0.25.

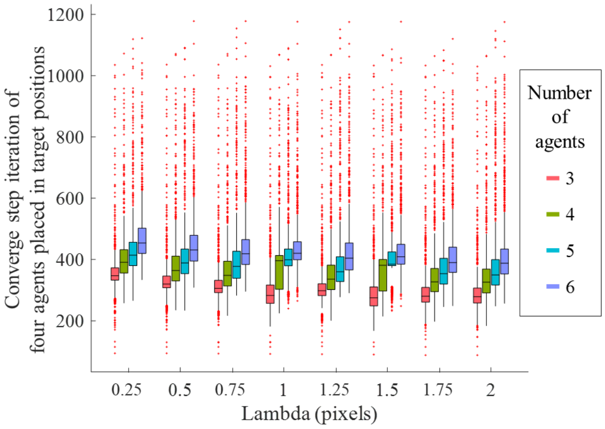

FIGURE 21. Required converge steps (0.02 s per step) of all agents for each number of agents according to each of the λ for round $L = 1000$. The boxed area represents 50% of the quantile of the cumulative error of angular velocity and red dots denote outlier samples beyond the box area. It can be known that as the λ grows, the converge time gets smaller.

B. POSITION AND ANGULAR FOLLOW-ABILITY OF IOCS METHOD

As expected, by using the IOCS strategy, the holonomic control method (OAFC method) is applied to nonholonomic agents in the experiment (Fig. 14). As shown in the result, to apply the IOCS method, the reference position frame should be computed in advance (Fig. 15). In the agent control experiment, both the absolute and angular errors between the desired positions and the angles of the agents converged to zero after 15 s (Fig. 16 and Fig. 19). However, by implementing the IOCS method to more high-performance designed robot agents, the converging time may be reduced with higher gains (Table 1). Therefore, the results show that by using the IOCS, other orientation alignment-based control strategies for holonomic systems can be applied to nonholonomic systems, such as a distributed consensus controller approach [26].

C. RELATIONSHIP BETWEEN λ AND CMAE

When applying the IOCS, the angle difference ψ is critical during the instant correction process because it is fundamental to follow the consensus frame (Fig. 18). Therefore, during the estimation of the absolute error between the orientation angle and nonholonomic frame, a bumping epoch, which can be interpreted as an inconstant angular velocity during agent control, was observed (Fig. 19). As expected, the bumping samples originated from the parameter λ (23). Particularly, regardless of the number of agents, the results of the CMAE analysis have shown that as λ increases, the cumulative mean angular velocity increases (Fig. 20). This is because λ is essentially an updated frequency of the intermediate frame ${}^{\ell}_{m}\Sigma$. Therefore, when applying the IOCS, a suitable value for λ should be set in advance for the precise control of multiple agents to prevent unstable angular outputs.

D. CONVERGE TIME TO TARGET POSITIONS

Contrarily, λ was relevant to the converging time to the desired points (Fig. 21). Notably, λ only contributes to the stability of angular control because the agents immediately change their intermediate frames when the distance of λ increases. Therefore, as λ decreases, the agents can precisely be controlled in angular and positional aspects. Conversely, when λ is unnecessarily small, local frames can be over-updated to degrade the performance of the convergence. In addition, depending on the number of agents, the sensitivity of converging time against λ was shown to be different. For instance, the mean coverage step iteration of agents when the number of agents was three was smaller than that of four. Therefore, following the usage of the IOCS, λ should be carefully chosen not to degrade the performance of the agent system considering the number of agents.

E. LIMITATIONS AND PRACTICAL FEASIBILITY

During the experiment of the agent control system, the OpenCV algorithm with the top-view camera was used to estimate the positions and orientations of each of the agents. However, due to the precision of the camera and the object detection algorithm, the error of positions and orientation angle remained for about 15 pixels, and ±0.3 radian (Fig. 16, and 16). On the other hand, because the uncertainty of object detection is not considered in the simulation results, it shows a relatively high alignment accuracy (Fig. 10). Therefore, when applying IOCS in an actual environment, it is important to accurately estimate their each location.

In addition, careful consideration should be given to the situation where implementing IOCS aligns various formations. Due to the non-holonomic constraints, orientation alignment is not guaranteed if the desired position is beyond the domain of dimensions. Therefore, desired position and target should be located in the domain of physically feasible boundaries to align the agents effectively. Furthermore, the agents are able to be located closely until each agent collides and is physically not disturbing. Therefore, an appropriate collision avoidance algorithm should be carefully adopted not to degrade the performance of the system.

VI. CONCLUSION

In this study, a correction method, the IOCS, for nonholonomic dynamics was proposed to perform a control law targeting holonomic agents using nonholonomic systems. The IOCS corrected local variables in a local frame used in a holonomic system-based control law by using the difference in the orientation angle between the local frames of nonholonomic agents and intermediate states. By using the IOCS, the divergence of variables due to the difference between the orientations of local frames was successfully removed and the result was verified by experiment and simulations with unicycle-modeled agents. Therefore, nonholonomic agents could execute a holonomic system-based control law by applying the proposed correction strategy.

REFERENCES

[1] K.-K. Oh, M.-C. Park, and H.-S. Ahn, "A survey of multi-agent formation control," *Automatica*, vol. 53, pp. 424–440, Mar. 2015.

[2] S.-M. Kang, M.-C. Park, B.-H. Lee, K.-K. Oh, and H.-S. Ahn, "Distance-based formation control: Background, principal results and issues," *J. Inst. Control, Robot. Syst.*, vol. 19, no. 5, pp. 398–409, May 2013.

[3] X. Ge, Q.-L. Han, D. Ding, X.-M. Zhang, and B. Ning, "A survey on recent advances in distributed sampled-data cooperative control of multi-agent systems," *Neurocomputing*, vol. 275, pp. 1684–1701, Jan. 2018.

[4] Y. Rizk, M. Awad, and E. Tunstel, "Decision making in multiagent systems: A survey," *IEEE Trans. Cognit. Develop. Syst.*, vol. 10, no. 3, pp. 514–529, Sep. 2018.

[5] Z. Lin, B. Francis, and M. Maggiore, "Necessary and sufficient graphical conditions for formation control of unicycles," *IEEE Trans. Autom. Control*, vol. 50, no. 1, pp. 121–127, Jan. 2005.

[6] L. Consolini, F. Morbidi, D. Prattichizzo, and M. Tosques, "Leader-follower formation control of nonholonomic mobile robots with input constraints," *Automatica*, vol. 44, no. 5, pp. 1343–1349, May 2008. [Online]. Available: https://www.sciencedirect.com/science/article/pii/S0005109807004578

[7] K. Listmann, M. Masalawala, and J. Adamy, "Consensus for formation control of nonholonomic mobile robots," in *Proc. IEEE Int. Conf. Robot. Automat.*, May 2009, pp. 3886–3891.

[8] T. Liu and Z.-P. Jiang, "Distributed formation control of nonholonomic mobile robots without global position measurements," *Automatica*, vol. 49, no. 2, pp. 592–600, Feb. 2013. [Online]. Available: https://www.sciencedirect.com/science/article/pii/S0005109812005675

[9] X. Liang, H. Wang, Y.-H. Liu, W. Chen, and T. Liu, "Formation control of nonholonomic mobile robots without position and velocity measurements," *IEEE Trans. Robot.*, vol. 34, no. 2, pp. 434–446, Apr. 2018.

[10] A. Saradagi, V. Muralidharan, V. Krishnan, S. Menta, and A. D. Mahindrakar, "Formation control and trajectory tracking of nonholonomic mobile robots," *IEEE Trans. Control Syst. Technol.*, vol. 26, no. 6, pp. 2250–2258, Nov. 2018.

[11] E. Montijano, E. Cristofalo, M. Schwager, and C. Sagues, "Distributed formation control of non-holonomic robots without a global reference frame," in *Proc. IEEE Int. Conf. Robot. Autom. (ICRA)*, May 2016, pp. 5248–5254.

[12] Q. Van Tran and H.-S. Ahn, "Distributed formation control of mobile agents via global orientation estimation," *IEEE Trans. Control Netw. Syst.*, vol. 7, no. 4, pp. 1654–1664, Dec. 2020.

[13] R. Olfati-Saber, J. A. Fax, and R. M. Murray, "Consensus and cooperation in networked multi-agent systems," *Proc. IEEE*, vol. 95, no. 1, pp. 215–233, Jan. 2007.

[14] Y. Quan Chen and Z. Wang, "Formation control: A review and a new consideration," in *Proc. IEEE/RSJ Int. Conf. Intell. Robots Syst.*, Aug. 2005, pp. 3181–3186.

[15] W. Ren, R. W. Beard, and E. M. Atkins, "A survey of consensus problems in multi-agent coordination," in *Proc. Amer. Control Conf.*, Jun. 2005, pp. 1859–1864.

[16] W. Ren, R. W. Beard, and E. M. Atkins, "Information consensus in multivehicle cooperative control," *IEEE Control Syst. Mag.*, vol. 27, no. 2, pp. 71–82, Apr. 2007.

[17] L. Krick, M. E. Broucke, and B. A. Francis, "Stabilisation of infinitesimally rigid formations of multi-robot networks," *Int. J. Control*, vol. 82, no. 3, pp. 423–439, 2009, doi: 10.1080/00207170802108441.

[18] K.-K. Oh and H.-S. Ahn, "Formation control of mobile agents based on inter-agent distance dynamics," *Automatica*, vol. 47, no. 10, pp. 2306–2312, Oct. 2011. [Online]. Available: http://www.sciencedirect.com/science/article/pii/S0005109811003906

[19] S.-M. Kang, J.-G. Lee, and H.-S. Ahn, "Shape and orientation control of moving formation with local measurements in three-dimensional space," in *Proc. IEEE Conf. Control Technol. Appl. (CCTA)*, Aug. 2018, pp. 1052–1057.

[20] K.-K. Oh and H.-S. Ahn, "Formation control and network localization via orientation alignment," *IEEE Trans. Autom. Control*, vol. 59, no. 2, pp. 540–545, Feb. 2013.

[21] K.-K. Oh and H.-S. Ahn, "Distance-based control of cycle-free persistent formations," in *Proc. IEEE Int. Symp. Intell. Control*, Sep. 2011, pp. 816–821.

[22] M. Basiri, A. N. Bishop, and P. Jensfelt, "Distributed control of triangular formations with angle-only constraints," *Syst. Control Lett.*, vol. 59, no. 2, pp. 147–154, Feb. 2010. [Online]. Available: http://www.sciencedirect.com/science/article/pii/S0167691109001595

[23] A. N. Bishop, I. Shames, and B. D. O. Anderson, "Stabilization of rigid formations with direction-only constraints," in *Proc. IEEE Conf. Decis. Control Eur. Control Conf.*, Dec. 2011, pp. 746–752.

[24] A. Franchi and P. R. Giordano, "Decentralized control of parallel rigid formations with direction constraints and bearing measurements," in *Proc. IEEE 51st IEEE Conf. Decis. Control (CDC)*, Dec. 2012, pp. 5310–5317.

[25] K. K. Oh and H. S. Ahn, "Formation control of mobile agents based on distributed position estimation," *IEEE Trans. Autom. Control*, vol. 58, no. 3, pp. 737–742, Mar. 2013.

[26] E. Montijano, D. Zhou, M. Schwager, and C. Sagues, "Distributed formation control without a global reference frame," in *Proc. Amer. Control Conf.*, Jun. 2014, pp. 3862–3867.

[27] K.-K. Oh and H.-S. Ahn, "Distributed formation control based on orientation alignment and position estimation," *Int. J. Control, Autom. Syst.*, vol. 16, no. 3, pp. 1112–1119, Jun. 2018.

[28] X. Yu and L. Liu, "Distributed formation control of nonholonomic vehicles subject to velocity constraints," *IEEE Trans. Ind. Electron.*, vol. 63, no. 2, pp. 1289–1298, Feb. 2015.

[29] C. Godsil and G. Royle, *Algebraic Graph Theory*. New York, NY, USA: Springer, 2001. https://books.google.co.kr/books?id=pYfJe-ZVUyAC

[30] M. W. Spong, S. Hutchinson, and M. Vidyasagar, *Robot Modeling and Control*, vol. 3. New York, NY, USA: Wiley, 2006.

[31] H.-S. Ahn, *Formation Control: Approaches for Distributed Agents* (Studies in Systems, Decision and Control), 1st ed. Springer, Apr. 2019. [Online]. Available: https://books.google.co.kr/books?id=RgMwxQEACAAJ

[32] F. C. Vieira, A. A. D. Medeiros, P. J. Alsina, and A. P. Araújo, "Position and orientation control of a two-wheeled differentially driven nonholonomic mobile robot," in *Proc. ICINCO*, vol. 2, 2004, pp. 256–262.

[33] G. Bradski and A. Kaehler, "OpenCV," *Dr. Dobb's J. Softw. Tools*, vol. 3, p. 120, 2000. [Online]. Available: http://roswiki.autolabor.com.cn/attachments/Events(2f)ICRA2010Tutorial/ICRA_2010_OpenCV_Tutorial.pdf

[34] E. Rublee, V. Rabaud, K. Konolige, and G. Bradski, "ORB: An efficient alternative to SIFT or SURF," in *Proc. Int. Conf. Comput. Vis.*, Nov. 2011, pp. 2564–2571.

[35] R. Wang, Y. Xia, G. Wang, and J. Tian, "License plate localization in complex scenes based on oriented FAST and rotated BRIEF feature," *J. Electron. Imag.*, vol. 24, no. 5, Sep. 2015, Art. no. 053011.

CHANYEONG JEONG was born in Daegu, South Korea, in 1996. He received the B.S. and M.S. degrees in mechanical engineering from the Gwangju Institute of Science and Technology, Gwangju, South Korea, in 2018 and 2020, respectively. He is currently with the Automotive Materials & Components Research and Development Group, Korea Institute of Industrial Technology. His research interests include control systems and autonomous vehicles.

EUGENE KIM was born in Busan, South Korea, in 1992. He received the B.S. degree in engineering from the Nagoya Institute of College, Nagoya, Japan, in 2016, and the M.S. and Ph.D. degrees in engineering from Nagoya University, Nagoya, in 2018 and 2021, respectively. He is currently with the Automotive Materials & Components Research and Development Group, Korea Institute of Industrial Technology. His research interests include functional/inherent safety of machinery, safety-related sensor systems, and automotive/remote driving vehicles.

MYEONG-HWAN HWANG received the Ph.D. degree in electrical engineering from Chonnam National University, South Korea, in 2021. He is currently with the Automotive Materials & Components Research and Development Group, Korea Institute of Industrial Technology. His research interests include hybrid electric vehicles (HEVs)/electric vehicles (EVs), and motor drive systems.

HYO-SUNG AHN (Senior Member, IEEE) received the B.S. and M.S. degrees in astronomy from Yonsei University, Seoul, South Korea, in 1998 and 2000, respectively, the M.S. degree in electrical engineering from the University of North Dakota, Grand Forks, in 2003, and the Ph.D. degree in electrical engineering from Utah State University, Logan, in 2006.

Since July 2007, he has been with the School of Mechatronics and the School of Mechanical Engineering, Gwangju Institute of Science and Technology (GIST), Gwangju, South Korea. Before joining the GIST, he was a Senior Researcher with the Electronics and Telecommunications Research Institute, Daejeon, South Korea. He is currently a Professor at the School of Mechanical Engineering, GIST. His research interests include distributed control, aerospace navigation and control, network localization, and learning control.

HYUN-ROK CHA received the Ph.D. degree in physics from the Tokyo Institute of Technology, Tokyo, Japan, in 2009. He was with the Samsung Electronics Research Center, Gwangju, for a period of four years. Since 2004, he has been a Senior Researcher with the Automotive Materials & Components Research and Development Group, Korea Institute of Industrial Technology. He is currently a Current Director of the Mobility Core Components and Materials Center, Seonam Division, Korea Institute of Industrial Technology, and a Professor at the University of Science and Technology. His research interests include e-mobility, electric vehicle (EV) platforms, smart vehicle control hybrid-powered drones, and power electronics.